

Forecasting high-resolution PM_{2.5} concentrations in southeastern China by combining high-resolution satellite data and numerical simulation with machine learning

Zeyue Li ^a , Yang Liu ^b, Jianzhao Bi ^c, Xuefei Hu ^{a,*}

^a School of Geospatial Engineering and Science, Sun Yat-sen University, Zhuhai, 519082, China

^b Gangarosa Department of Environmental Health, Rollins School of Public Health, Emory University, Atlanta, GA, 30322, USA

^c Department of Environmental & Occupational Health Science, University of Washington, Seattle, WA, 98105, USA

HIGHLIGHTS

- The proposed model integrated with satellite data outperforms the GEOS-CF model.
- Incorporating satellite data enhances the spatial resolution of PM_{2.5} forecasts.
- The proposed model captures the dynamics of PM_{2.5} pollution for the next five days.

ARTICLE INFO

Keywords:

PM_{2.5}
Air pollution forecast
Chemical transport model
MAIAC AOD
And random forest

ABSTRACT

PM_{2.5} is a significant air contaminant that presents a serious risk to human health. Accurate PM_{2.5} forecasts with high spatial resolution are essential for decision-makers to implement effective mitigation strategies and prevent harmful public exposure to PM_{2.5}. Current methods often rely on spatial data of limited precision, like outputs from spatial interpolation and chemical transport models (CTMs), resulting in PM_{2.5} forecasts that either have inaccurate spatial patterns or completely omit spatial details. For this research, we developed a novel approach to demonstrate the feasibility of employing 1 km satellite AOD data to generate 1 km resolution PM_{2.5} forecasts in southeastern China up to five days in advance by integrating machine learning models, CTM simulations, and 1 km resolution satellite AOD measurements. Our forecast framework integrated with satellite AOD data demonstrated superior performance, surpassing the precision of the original CTM forecast data, as evidenced by both spatial cross-validation and overall validation results. In addition, incorporating satellite AOD into the forecasting model could enhance the spatial resolution of PM_{2.5} forecasts. The model enables the production of PM_{2.5} forecasts featuring both accurate spatial representation and high spatial resolution.

1. Introduction

PM_{2.5}, which can be inhaled, is a significant air contaminant that presents a serious risk to human health worldwide (Lim et al., 2020). Epidemiological research has established a significant connection between prolonged exposure to PM_{2.5} pollution and a heightened likelihood of premature mortality from conditions such as cardiovascular diseases (Hayes et al., 2019), stroke (Yang et al., 2021b), respiratory illnesses (Zhang et al., 2022), and lung cancer (Cao et al., 2018), significantly impacting life expectancy (Apte et al., 2018). PM_{2.5} has caused the substantial degradation of air quality in China. According to

the Global Burden of Disease (GBD) study, China experienced an escalation in the average PM_{2.5} pollution level, rising from 48.5 to 58.4 µg/m³ between 1990 and 2015. This rise in pollution was mirrored by a corresponding uptick in mortality associated with PM_{2.5} exposure, which went up from 0.95 million to 1.11 million per year (Cohen et al., 2017). Therefore, near-term PM_{2.5} forecasts are essential for environmental agencies, offering the crucial data for the timely issuance of pollution warnings and the development of robust mitigation measures.

Timely and accurate PM_{2.5} concentration forecasting is vital but faces significant obstacles. Progress towards addressing this issue has led to the development of three key strategies. The initial approach involves

* Corresponding author.

E-mail address: huxf9@mail.sysu.edu.cn (X. Hu).

utilizing machine learning algorithms to forecast the temporal dynamics, specifically time series patterns, of PM_{2.5} levels at single air quality monitoring sites. Typical sequential machine learning models include three key recurrent neural network (RNN) architectures, encompassing the standard RNN, gated recurrent unit (GRU), and long short-term memory (LSTM) networks. These models leverage their exceptional prediction accuracy to derive highly reliable PM_{2.5} forecasts (Chang et al., 2020; Feng et al., 2019; Hu et al., 2024; Huang et al., 2021; Lin et al., 2024). Other involved machine learning techniques comprise support vector machine (SVM) (Ameri et al., 2023; Zhou et al., 2019), convolutional neural networks (CNN) (Kow et al., 2020; Lee et al., 2024), back propagation neural networks (BPNN) (Yang et al., 2021a), and support vector regression (SVR) (Abouelezz et al., 2025; Liu et al., 2017). However, these models can only forecast future PM_{2.5} levels at these existing monitoring sites and are unable to forecast the spatial patterns of PM_{2.5} levels (Feng et al., 2024).

Forecasting spatiotemporal patterns of PM_{2.5} concentrations at ground level can be accomplished by utilizing advanced numerical air quality models, referred to as chemical transport models (CTMs). CTM forecasts of PM_{2.5} concentrations typically range from hours to days and are widely available from various sources, including global numerical models like NASA's Goddard Earth Observing System Composition Forecast (GEOS-CF) (Keller et al., 2021) and the Copernicus Atmosphere Monitoring Service (CAMS) (Gualtieri et al., 2025; Wu et al., 2020). Regional air quality systems, encompassing the Comprehensive Air Quality Model with Extensions (CAMx) (Lu et al., 2021), the Nested Air Quality Prediction Modeling System (NAQPMS) (Liao et al., 2024; Zheng et al., 2018), and the Community Multiscale Air Quality Modeling System (CMAQ) (Cheng et al., 2021), also provide PM_{2.5} forecasts. Nevertheless, significant discrepancies exist between CTM forecast data and observations, primarily attributed to uncertainties in atmospheric chemical mechanisms, emission inventories, resolution, and meteorological conditions (Gao and Zhou, 2024). In addition, CTM forecast products currently fall short of providing precise, kilometer-scale forecasts aligned with ground reality (Bi et al., 2022). The complexity of solving multiple differential equations simultaneously leads to high computational costs for CTMs (Xing et al., 2022).

Another approach involves creating a hybrid methodology that integrates numerical simulation techniques with machine learning algorithms, effectively serving as a refinement process to improve the precision of PM_{2.5} forecasts derived from CTMs (Feng et al., 2024; Wu et al., 2020; Zhao et al., 2025). For example, Bi et al. (2022) proposed a PM_{2.5} forecast model by integrating the GEOS-CF forecast product with the random forest algorithm. The forecasting framework can generate spatiotemporally continuous PM_{2.5} forecasts for the upcoming five days with 1 km spatial resolution. They employed a current-day convolutional layer generated by ordinary kriging as an independent spatiotemporal predictor and found that the convolutional layer is a significant predictor in the model training process, especially for the first two days.

Previous research has some drawbacks. One key issue is that these studies often forecasted changes in PM_{2.5} levels across different locations using unreliable spatial information, often sourced from methods like CTM simulations or geographical interpolation. To address this issue, a common approach for predicting spatial patterns of PM_{2.5} levels involves utilizing satellite retrievals of aerosol optical depth (AOD) (He et al., 2023; Hu et al. 2013, 2017; Ma et al., 2014; Wei et al. 2021, 2023). Satellite AOD-derived PM_{2.5} concentrations using machine learning models are generally more accurate than those obtained through spatial interpolation or CTM simulations (Handschtuh et al., 2024; Jin et al., 2019). Furthermore, it is possible to estimate ground-level PM_{2.5} concentrations with high spatial resolution using high-resolution satellite AOD data (He et al., 2023; Hu et al., 2014; Wei et al. 2021, 2023; Xiao et al., 2017). As a result, integrating high-resolution satellite AOD data into forecasting models could offer a significant opportunity to improve spatial understanding of PM_{2.5} patterns and boost the overall precision

and resolution of PM_{2.5} forecasts. While promising, the application of satellite AOD in forecasting models has not been fully realized, with current efforts remaining somewhat limited (Jena et al., 2021; Teng et al. 2023, 2024). To date, it is still a challenge to incorporate satellite AOD into a forecast model, and the impact of satellite AOD on the accuracy of PM_{2.5} forecasts has not been comprehensively examined.

For this research, we aim to demonstrate the feasibility of utilizing 1 km satellite AOD data to forecast 1 km resolution PM_{2.5} concentrations with high precision for the upcoming five days. We first construct a 1 km resolution convolutional layer representing present-day PM_{2.5} levels for each day utilizing satellite AOD, meteorological fields, and land use variables as input features, with ground PM_{2.5} measurements serving as the target variable. Subsequently, we develop separate forecast models for each day within the five-day forecast horizon. The convolutional layers, GEOS-CF PM_{2.5} and meteorological forecasts, and land use variables were integrated into a random forest (RF) forecasting framework as input features, with ground PM_{2.5} measurements serving as the target variable. We anticipate that our model can yield a precise spatial representation of PM_{2.5} forecasts with high resolution due to the additional spatial insights that high-resolution satellite data introduces into the model. To avoid model overfitting, our model training and validation processes exclude future PM_{2.5} observations, ensuring reliable forecasting of PM_{2.5} levels.

2. Materials and methods

This research concentrated on the southeastern region of China (Fig. 1), covering the provinces of Hunan, Jiangxi, Fujian, Zhejiang, and Guangdong. This region was chosen for its significant challenges related to PM_{2.5} pollution.

2.1. Ground PM_{2.5} observations

We collected hourly in situ ground-level PM_{2.5} measurements from 375 air quality monitors in southeastern China, spanning from September 01, 2022, to January 10, 2024, sourced from the China National Environmental Monitoring Center (CNEMC, <https://air.cnemc.cn:18007/>). Fig. 1 displays the monitoring site locations within the study region. To establish the dependent variable for our forecast model, we derived daily mean PM_{2.5} concentrations by averaging the hourly PM_{2.5} measurements from each monitoring site.

2.2. Satellite AOD data

This study utilized the AOD product obtained through the Multi-Angle Implementation of Atmospheric Correction (MAIAC) algorithm (Lyapustin et al. 2011a, 2011b). We obtained MAIAC AOD data for the study area spanning from September 01, 2022, to January 10, 2024, through the Land Processes Distributed Active Archive Center (<https://lpdaac.usgs.gov/>). AOD data were retrieved at 550 nm, along with quality assurance flags. These quality flags were utilized to filter out any invalid AOD measurements. For the purpose of data integration, we employed the 1-km grid provided by the MAIAC dataset. To fill the gaps caused by missing MAIAC AOD data, we employed the GEOS-CF hourly-average column total AOD at 550 nm, and missing MAIAC AOD was estimated from GEOS-CF AOD by implementing the model proposed by Stafoggia et al. (2019). The model was fitted daily using a five-day rolling window, incorporating data from two preceding days, the modeling day, and two subsequent days (Xiao et al., 2017). We validated our daily gap-filling method using 10-fold cross-validation (CV), which yielded daily CV R^2 values ranging from 0.23 to 0.94, with a mean of 0.76, indicating generally reasonable performance.

2.3. CTM-based PM_{2.5} forecast data

Freely available PM_{2.5} forecasts were obtained from the Goddard

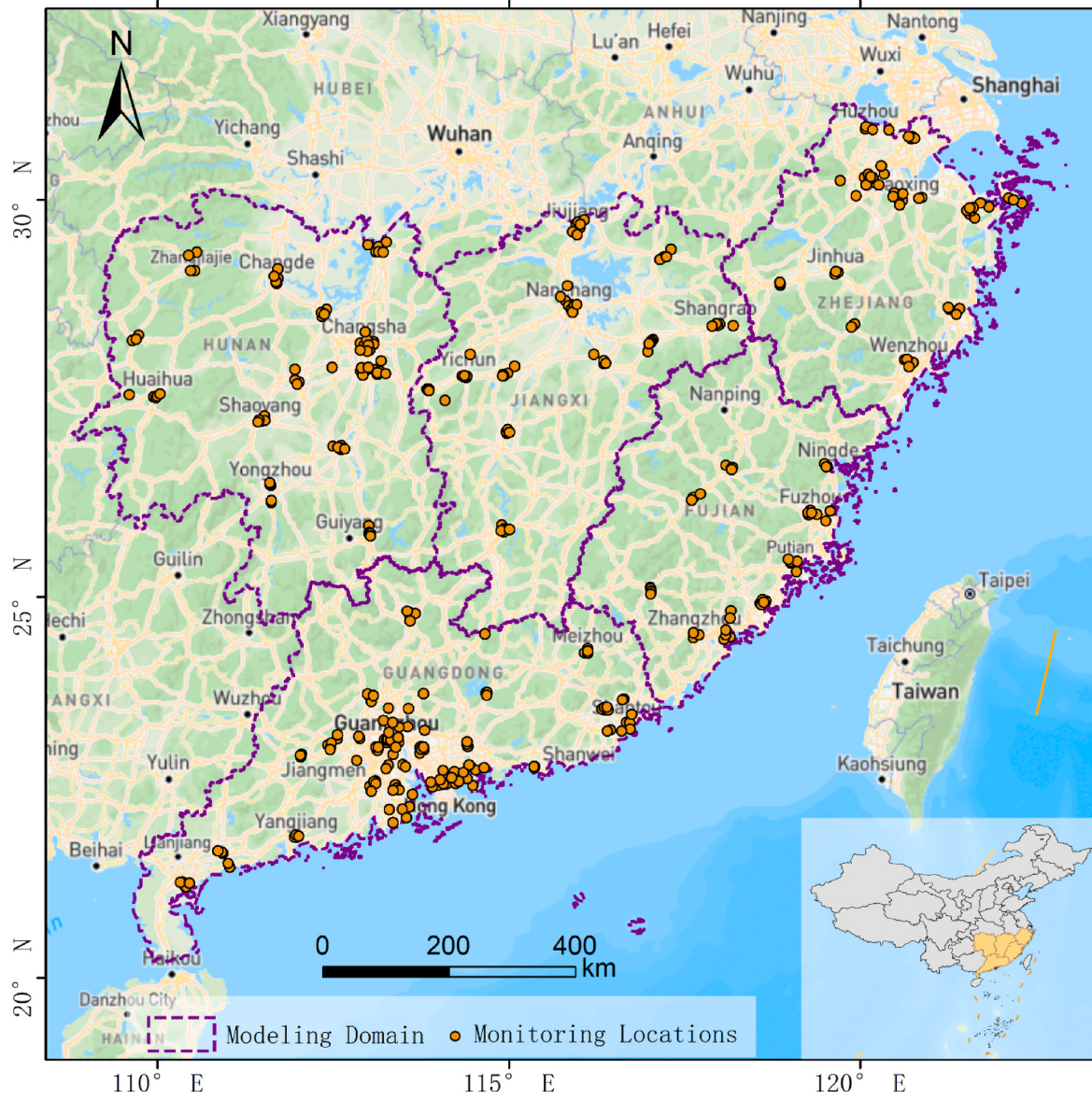


Fig. 1. Study area.

Earth Observing System “Composition Forecasting” (GEOS-CF) database (<https://gmao.gsfc.nasa.gov/>). GEOS-CF is a pioneering meteorology and atmospheric composition model developed by the National Aeronautics and Space Administration (NASA). The GEOS-CF system, powered by the GEOS-Chem model (<https://www.geos-chem.org>), delivers daily forecasts of global atmospheric composition (including NO₂, ozone, and PM_{2.5}) at a 25 km resolution, and these operational forecasts extend 5 days into the future and are available in near-real-time (Knowland et al., 2022). GEOS-CF tends to overpredict the ground-level PM_{2.5} levels, with the most significant discrepancies observed in Asia. While GEOS-CF's PM_{2.5} data exhibits systematic biases, it successfully captures the general spatial distributions of PM_{2.5} concentrations. This suggests that the model is effective in replicating the overall geographical trends of PM_{2.5}, despite some inaccuracies in the absolute values (Keller et al., 2021). In this research, we determined daily mean PM_{2.5} concentrations for the five forecast days using the two-dimensional surface-level GEOS-CF forecast data, calibrated according to the China Standard Time (CST), equivalent to the GMT+8 time zone. It should be noted that forecast data encompassing a full 24-h period was available for days one through four. Day five featured a 21-h

forecast, commencing at 12 a.m. and concluding at 8 p.m. CST. We then resampled all the PM_{2.5} forecast data to the MAIAC grid at 1 km resolution.

2.4. Meteorological forecast data

We acquired meteorological fields at the surface level covering the five forecast days from GEOS-CF. The meteorological variables used in the model comprise planetary boundary layer height (m), surface skin temperature (K), tropopause pressure based on blended estimate (Pa), total precipitation (kg/m²/s), 10 m air temperature (K), 10 m specific humidity (kg/kg), surface pressure (Pa), total cloud area fraction (unitless), and 10 m eastward/northward wind (m/s). Daily mean meteorological variables were calculated and employed in the forecast framework to capture the spatiotemporal variability in PM_{2.5} levels. We then resampled all the meteorological fields into the MAIAC grid at 1 km resolution.

2.5. Land-use data

We employed spatially varying land-use factors as predictors in our forecast model to capture the spatial variations in PM_{2.5} levels. Those variables comprise primary and secondary road lengths extracted from the OpenStreetMap (OSM) road network data (<https://www.openstreetmap.org>), the LandScan ambient population in 2022 at a spatial resolution of 900m (<https://landscan.ornl.gov>), and the percentages of vegetation, water, and urban cover calculated from the Copernicus Climate Change Services (C3S) global Land Cover (LC) products in 2018 at a spatial resolution of ~300m (<https://cds.climate.copernicus.eu/>). We then resampled all these land use variables to the MAIAC grid at 1 km resolution.

2.6. Forecast model training and prediction

Our forecasting framework consists of two main steps. Initially, we create a 1 km resolution convolutional layer for each day using MAIAC AOD, meteorological fields, and land use variables as input features, with ground PM_{2.5} measurements serving as the training label. Subsequently, we develop separate forecast models for each of the five forecast days. For these models, we utilize the convolutional layers, GEOS-CF PM_{2.5} and meteorological forecasts, and land use variables as input features, while ground PM_{2.5} measurements are used as the training label. Fig. S1 outlines the stages of our forecast modeling and validation approach, along with relationships among various data. Our forecasting framework is built on the RF algorithm, which constructs an ensemble of decision trees and provides insights into the relative contribution of each predictor variable to the overall prediction accuracy. The RF model has become increasingly popular owing to its outstanding predictive performance, effective handling of complex, multi-feature datasets, and straightforward implementation process (Hu et al., 2017). Bi et al. (2022) compared the forecast performance of the RF and XGBoost models and revealed that while RF marginally outperformed XGBoost, the difference between the two was negligible. Their selection of the RF algorithm was guided by its ease of configuration, requiring fewer major hyperparameters, and its capacity for robust predictions without extensive tuning. As the primary objective of this research is to explore the potential of using 1 km satellite AOD data to accurately forecast PM_{2.5} concentrations at a 1 km resolution over a five-day period, we extend their work by incorporating satellite AOD data into their proven RF forecasting framework. This design allows us to directly compare with their original approach and evaluate the role of satellite AOD data in forecasting. Although other machine learning models might outperform the RF model, our focus remains on the satellite data integration methodology itself. Consequently, the RF model was selected in this study as a suitable choice. During the training phase of the RF model, two critical hyperparameters must be specified: the number of predictors randomly tried at each split (m_{try}) and the number of decision trees (n_{tree}). We developed a current-day PM_{2.5} prediction model. This model is not for forecasting but rather to facilitate predictor selection and hyperparameter tuning. The model utilizes ground-level PM_{2.5} observations as the dependent variable and employs the same-day meteorological fields from GEOS-CF and land-use factors as predictor variables. By using the current-day model, we can fine-tune the model's hyperparameters, identify the most relevant predictors, and optimize the model's performance before applying it to forecasting tasks. This approach helps to ensure that the final forecast model is accurate, efficient, and robust. Through our analysis, we identified optimal values for n_{tree} and m_{try} , which were found to be 500 and 5, respectively. Furthermore, we utilized RF variable importance estimates to inform our selection of predictors for the forecast model, omitting any variables with significantly lower importance values compared to others.

To ensure that the forecast model accurately reflects real-world conditions, we designed it to avoid using future data during the training phase and construct the forecasting model for each forecast day

separately using a rolling method. For example, the first-day model is designed to predict PM_{2.5} levels for the following day, while the second-day model is intended to predict PM_{2.5} concentrations two days in advance. Similarly, the third-day model is designed to predict PM_{2.5} levels three days ahead, the fourth-day model is intended to predict PM_{2.5} concentrations four days in advance, and the fifth-day model aims to predict PM_{2.5} levels five days into the future. To determine the best rolling period for achieving the highest level of forecast accuracy, we experimented with several different durations, including 10, 30, 60, and 90 days. In the process of model training, we utilized a unique approach. In the first-day model with a 10-day rolling period, the dependent variable comprised PM_{2.5} observations across a 10-day window, from day -9 to day 0. The predictors consisted of GEOS-CF meteorological and PM_{2.5} first-day forecasts spanning from day -10 through day -1. In the model forecasting step, we utilized GEOS-CF meteorological and PM_{2.5} first-day forecasts from day 0 to predict PM_{2.5} concentrations on the subsequent day, day 1. Based on a comparison of model performance, we found that a rolling period of 60 days was optimal (Table S1). The specific approach used to construct each day's forecast model is outlined in Table 1.

2.7. The construction of the convolutional layer

As an additional spatiotemporal predictor in our model, we constructed a PM_{2.5} convolutional layer that captured spatiotemporal patterns. In previous modeling studies, the PM_{2.5} convolutional layer has been frequently employed as a predictor of PM_{2.5} exposure (Bi et al., 2022). With the addition of the PM_{2.5} convolutional layer, our forecast models were able to take into account the spatiotemporal correlations of PM_{2.5} concentrations, including those between adjacent locations and across current and forecast periods. The present-day convolutional layer was produced by integrating MAIAC AOD data into the RF model to build a present-day PM_{2.5} predictive model (Hu et al., 2017) (hereafter referred to as the RF convolutional layer). This model integrates various data sources, including PM_{2.5} ground measurements, MAIAC AOD data, land-use variables, and meteorological fields. By training the model on this comprehensive dataset, it can learn patterns and relationships to make more accurate present-day PM_{2.5} predictions. To understand how each input feature influenced the model's predictions, we employed the Shapley Additive Explanations (SHAP) method. Analysis of the mean absolute SHAP values (Fig. S2) revealed that MAIAC AOD observations were among the top three most influential factors in the PM_{2.5} prediction. Our forecast framework (hereafter termed our MAIAC model) employed the RF convolutional layer generated using the MAIAC AOD data as a spatiotemporal predictor.

2.8. Forecast model validation

To ensure the accuracy and reliability of our forecast models, we employed a robust validation process. Specifically, we compared our predicted PM_{2.5} levels with ground in situ observations, providing an out-of-sample evaluation method. This crucial step ensured that the model was not trained on the data it was intended to predict and generated an out-of-sample evaluation dataset, offering an impartial validation of the models' performance. Based on the out-of-sample validation dataset, our validation approach included three distinct schemes: an overall validation to assess the models' general accuracy, a site-specific evaluation to examine their effectiveness at each monitoring station, and a day-specific assessment to evaluate their effectiveness on a daily basis throughout the forecast period. To quantify the accuracy of our forecast models, we employed a range of out-of-sample validation metrics, such as normalized mean bias (NMB), the coefficient of determination (R^2), mean absolute percentage error (MAPE), and root-mean-square error (RMSE) (Eqs. S1-S4). In addition, we performed a 10-fold spatial cross-validation (CV) to evaluate the reliability of our predictions in regions without ground monitoring data. We first divided

Table 1

Forecast model building process by matching ground PM_{2.5} observations with the convolutional layer and GEOS-CF forecast data (PM_{2.5} pollution and meteorology forecast) as training and prediction data^a.

Forecast Day	Day of the Convolutional Layer	Training		Prediction	
		CTM Running Day	PM _{2.5} Observations and CTM Forecast Day	CTM Running Day	CTM Forecast Day
Day 1	Day 0	Day -N to -1	Day -(N-1) to 0	Day 0	Day 1
Day 2		Day -(N+1) to -2			Day 2
Day 3		Day -(N+2) to -3			Day 3
Day 4		Day -(N+3) to -4			Day 4
Day 5		Day -(N+4) to -5			Day 5

^a N is the rolling period (N = 60 days). Day 0 is the present day, Day 1 is the next day, etc.

the ground monitors into 10 subsets of roughly equal size through random allocation. In each round of the CV process, nine subsets were dedicated to training the model, and one subset was reserved for independent testing. We repeated this process 10 times, with a different subset used for testing each time.

3. Results

3.1. Overall and spatial CV validation

Table 2 presents the overall performance evaluation for our MAIAC model and the GEOS-CF model. The evaluation period spans from January 01, 2023, to December 31, 2023, and the results are presented for each of the five forecast days. Our MAIAC model exhibited superior performance compared to the GEOS-CF model throughout all five forecast days, with significant enhancements observed in all validation metrics. In addition, as we moved further into the forecast period, from day 1 through day 5, our models' performance declined, marked by a decrease in R² and increases in both RMSE and MAPE, suggesting a degradation in predictive accuracy over time. **Fig. S3** displays the spatial distribution of the 95 % confidence interval (CI) widths for our forecasts, which are comparable to the RMSE values and generally show an increasing trend over the five-day period. The spatial patterns reveal that the 95 % CI widths are larger in the northern part of the study area, particularly in Hunan Province, and smaller in the southern regions. This pattern may be attributed to PM_{2.5} pollution transported from outside the study domain—primarily from northern China—which may not have been fully captured by our model.

Fig. 2 illustrates the comparisons of PM_{2.5} ground measurements with forecasts from (a) the GEOS-CF model and (b) our MAIAC model. The results demonstrated that our MAIAC model with the RF convolutional layer substantially outperformed the initial GEOS-CF model with significantly improved validation metrics. The visual analysis demonstrated that the forecasts generated by our MAIAC model exhibited a stronger correlation with the observed values. This was demonstrated

through a regression line that nearly resembled the perfect 1:1 ratio, suggesting that our MAIAC model achieved a superior level of precision in its predictions. It is noted that PM_{2.5} forecasts from the GEOS-CF model exhibit a substantial overestimation when compared to ground observations, indicating a significant disagreement between the model's predictions and real-world measurements (Keller et al., 2021). However, moderate linear relationships between the GEOS-CF PM_{2.5} forecasts and in-situ measurements can be observed across the five forecasting days. All days exhibited correlation coefficient values greater than 0.63, indicating systematic biases existing within the initial GEOS-CF PM_{2.5} forecasting results.

Table 3 presents the results of the 10-fold spatial CV of our MAIAC model over the one-year period. To maintain consistency, the spatial CV procedure utilized the same modeling dataset as the overall validation. In each round of the spatial CV, the model was trained on nine subsets of the data, with one subset reserved for testing. Spatial CV results were consistent with the overall validation, showing similar performance patterns. However, notable discrepancies between overall validation and spatial CV were observed in slightly decreased R² values, marginally increased MAPE and RMSE, and comparable NMB values. In a direct comparison with the GEOS-CF model, the spatial CV results of our MAIAC model showed a significant performance improvement compared to the GEOS-CF model's validation results across all five forecast days, indicating a consistent enhancement by our MAIAC model in forecasting spatial patterns of PM_{2.5} levels.

3.2. Variable importance evaluation

Fig. 3 illustrated the relative contribution of different variables to our forecast model, broken down by each of the five days included in the forecast. The RF convolutional layer and the GEOS-CF PM_{2.5} forecasts emerged as the top two most important variables over the five-day forecast period. Specifically, the RF convolutional layer demonstrated the highest importance on the first forecasting day and held second place for the remaining four days, reflecting a persistent and strong association between today's PM_{2.5} concentrations and the forecasted PM_{2.5} levels for the next five days. The GEOS-CF PM_{2.5} forecasts, on the other hand, rank second in importance for the first forecasting day and remain first for the rest four days. As expected, even with their inherent biases, the GEOS-CF PM_{2.5} forecasts exhibit relatively strong correlations with ground in situ PM_{2.5} measurements, as evidenced by correlation coefficients above 0.63 for the entire 5-day forecasting period. Other important variables include 10m specific humidity and total cloud area fraction. Humidity has been identified as one of the pivotal meteorological variables in predicting PM_{2.5} levels (Peng et al., 2022), and there is a significant inverse relationship between cloud cover and PM_{2.5} concentrations (Yu et al., 2015). In addition, it should be noted that meteorological variables held greater significance compared to land-use variables, suggesting that these spatiotemporal variables made larger contributions to the forecasting results. While this study's land-use variables are static over time and primarily reflect local emission sources, ambient PM_{2.5} is a complex mixture affected by both local sources and regional transport largely driven by meteorological conditions,

Table 2

Overall validation performance of our MAIAC model and the GEOS-CF model for the period from January 01, 2023 to December 31, 2023^a.

Forecast Day	N of the Test Sample	R ²	RMSE ($\mu\text{g}/\text{m}^3$)	MAPE (%)	NMB (%)
Our MAIAC					
Day 1	133540	0.7142	10.7841	33.94	-0.21
Day 2	133535	0.6407	12.0834	38.53	-0.72
Day 3	133530	0.6142	12.4719	40.53	-0.59
Day 4	133526	0.5995	12.6580	42.16	-0.50
Day 5	133522	0.5591	13.1712	43.70	-0.79
GEOS-CF					
Day1	133540	-12.2363	73.3948	246.24	195.12
Day2	133535	-12.2411	73.3495	241.47	190.17
Day3	133530	-12.4421	73.6145	244.55	190.04
Day4	133526	-13.0211	74.8923	250.99	193.94
Day5	133522	-13.7423	76.1654	259.17	196.98

^a The rolling period was 60 days.

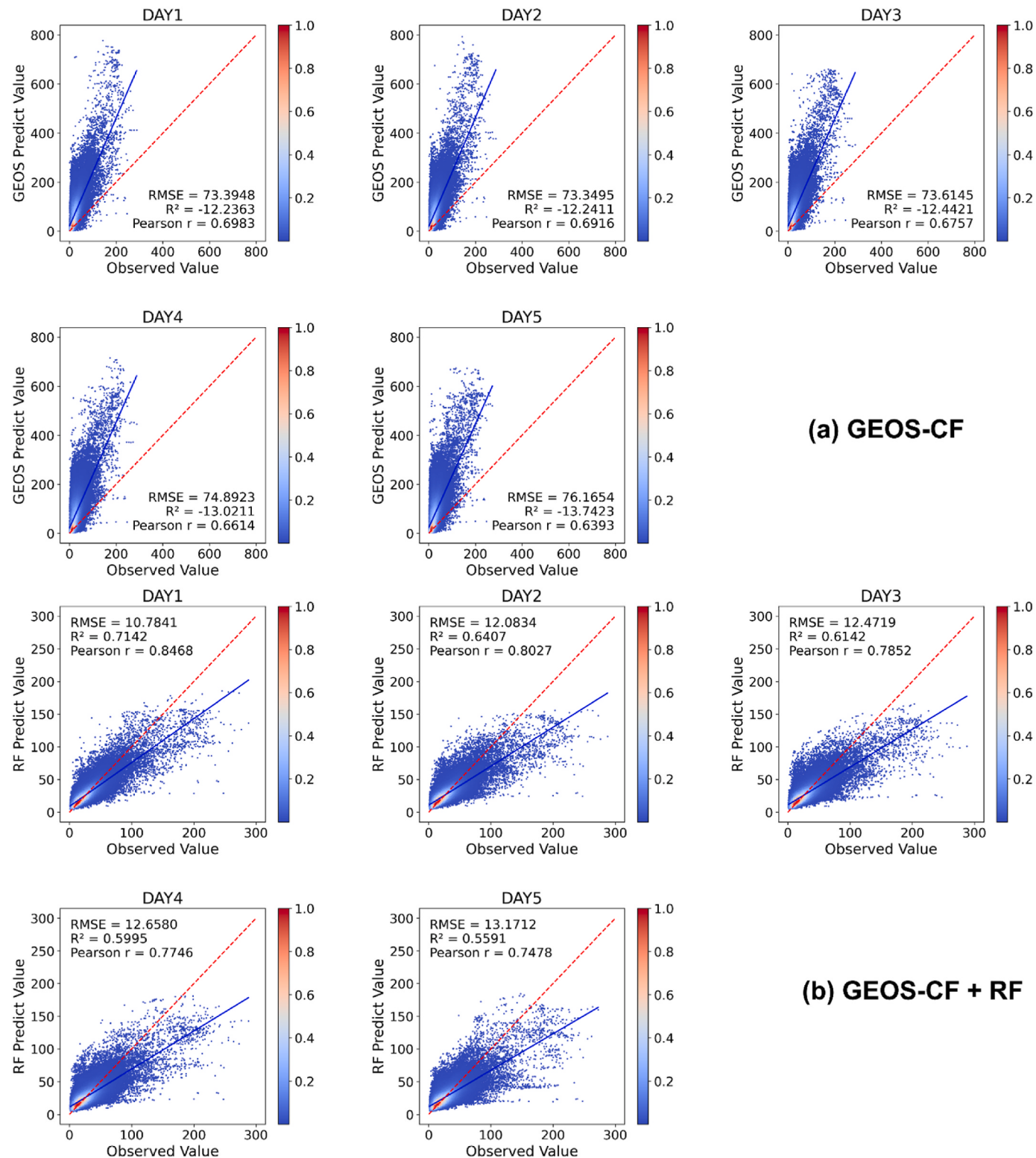


Fig. 2. Scatter plots between observed values and model forecasts for (a) the GEOS-CF model and (b) our MAIAC model (GEOS-CF + RF).

leading to significant spatiotemporal variations in PM_{2.5} concentrations (Chen et al., 2021). This means static land-use variables may struggle to capture the PM_{2.5} variations resulting from regional transport, limiting their predictive power in our model. In contrast, the model's MAIAC-based convolutional layers that utilize additional spatiotemporal information from MAIAC AOD data, coupled with GEOS-CF PM_{2.5} and meteorological forecasts, offer a dynamic perspective, capturing

both spatial variations and temporal fluctuations in PM_{2.5} levels, thereby improving the model's ability to account for regional transport.

3.3. Site-specific and day-specific validation

Fig. 4 presents the validation results specific to each (a) day and (b) site across the five-day forecast period separately for our MAIAC model

Table 3

Tenfold spatial CV performance of our MAIAC model for the period from January 01, 2023 to December 31, 2023^a.

Forecast Day	N of the Test Sample	R ²	RMSE ($\mu\text{g}/\text{m}^3$)	MAPE (%)	NMB (%)
Day 1	133540	0.7011	11.0295	35.45	0.34
Day 2	133535	0.6287	12.2826	40.03	-0.15
Day 3	133530	0.6014	12.6762	42.93	-0.10
Day 4	133526	0.5821	12.9293	43.58	-0.12
Day 5	133522	0.5440	13.3954	45.06	-0.50

^a The rolling period was 60 days.

and the GEOS-CF model. Significant superiority in forecast accuracy was observed with our MAIAC model when compared to the GEOS-CF model, according to the results.

In particular, the site-specific validation results indicated that our MAIAC model exhibited notably better performance than the original GEOS-CF model. This was evidenced by higher R², lower MAPE and RMSE values, and NMB scores that were nearing zero. Specifically, our MAIAC model's median R² values over the five-day forecast period fluctuated between 0.44 and 0.64, whereas the GEOS-CF model's corresponding values are all in negative territory, indicating significantly enhanced performance of our MAIAC model. Furthermore, the interquartile ranges (IQR) for R² of our MAIAC model were more constrained compared to those of the GEOS-CF model over the five days of forecasting. The narrower distribution of this metric underscores the reliability and stability of our MAIAC model.

In terms of the day-specific validation, our MAIAC model maintained a steady performance advantage over the GEOS-CF model,

demonstrating superior accuracy across multiple metrics, including higher R², lower MAPE and RMSE values, and NMB results that approached zero more closely. Much like the site-specific evaluation, the day-specific evaluation outcomes also depict narrower IQRs for R² across all five forecast days, demonstrating enhanced model reliability and consistency against the GEOS-CF model. It is observed that the day-specific evaluation yielded a broader range of R² values, displaying wider IQRs compared to those observed in the site-specific evaluation. This indicates that our MAIAC model encounters greater challenges in predicting the spatial variations in PM_{2.5} levels for a specific day than it does in forecasting temporal changes for a specific monitor station, a finding in line with prior studies (Bi et al., 2022).

Fig. 4c illustrates the variations in MAPE values assessed through day-specific evaluation for the first day of forecasting, along with the daily PM_{2.5} levels, spanning from January 01, 2023, to December 31, 2023. The results indicate that MAPE generally increased after a substantial drop in PM_{2.5} levels, suggesting that our MAIAC model's forecasting accuracy diminishes under these circumstances. This phenomenon was also observed by Bi et al. (2022).

3.4. Spatial distributions of PM_{2.5} forecasts during special events

Fig. 5 displays the spatial distributions of the 5-day PM_{2.5} forecasts derived from (a) our MAIAC model and (b) the GEOS-CF model on January 21, 2023, one day prior to the Lunar New Year holiday week. As shown in Fig. 5a, the PM_{2.5} forecasts from our MAIAC model reveal a peak in PM_{2.5} levels on the first day of the Lunar New Year holiday week, likely attributed to increased emissions from human activities and fireworks, followed by a gradual decline over the subsequent four days.



Fig. 3. Variable importance values across the five forecast days for the forecasting framework.

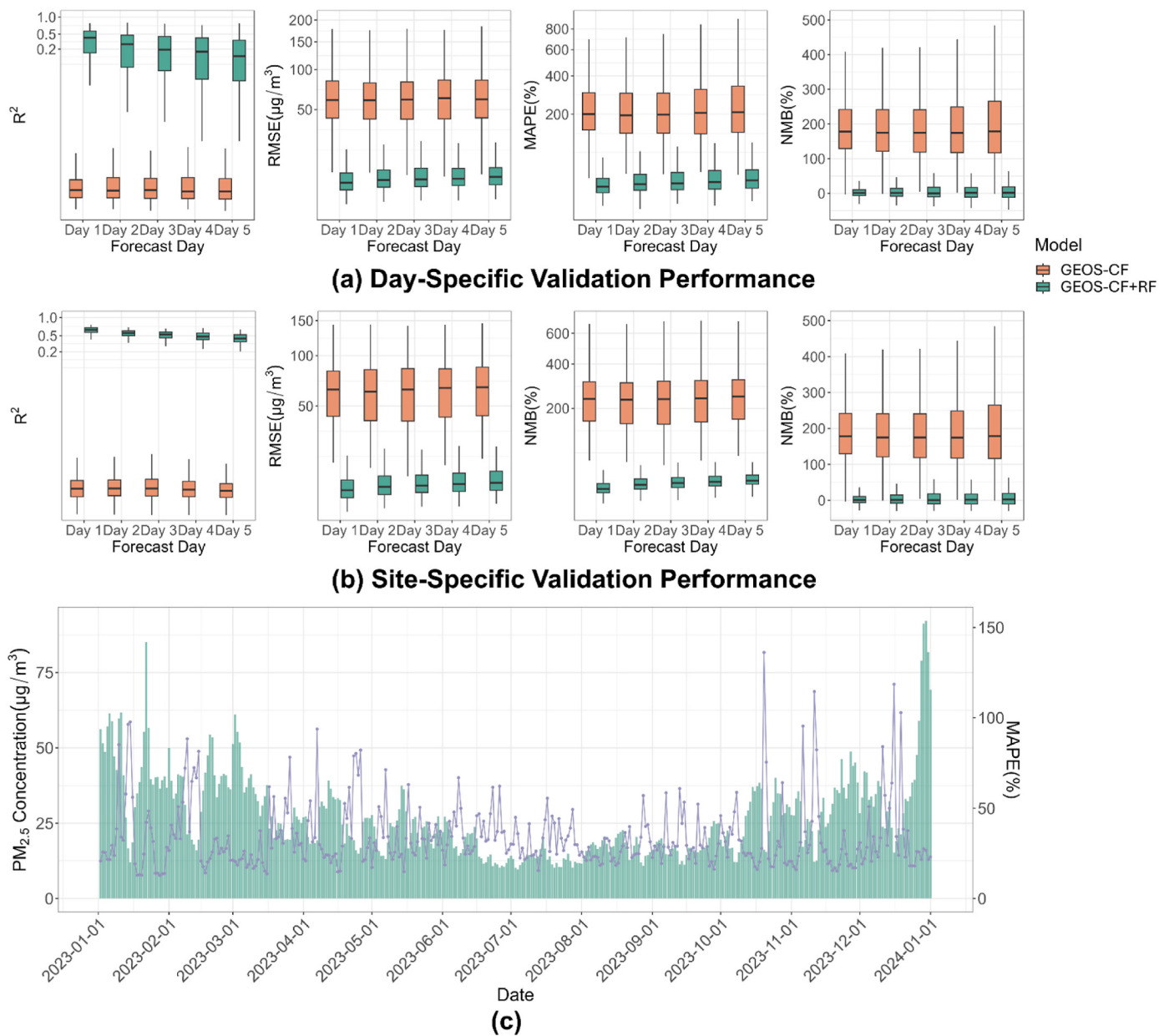


Fig. 4. (a) Day-specific and (b) site-specific validation performance. (c) Daily validation MAPE values (blue dots) with domain-average PM_{2.5} concentrations (green bars) using the first forecast day as an example.

Notably, this forecasted trend is well corroborated by ground-based measurements, indicating strong agreement between our MAIAC model's forecasts and actual observations. Conversely, the GEOS-CF forecasts (Fig. 5b) fail to capture this trend, instead forecasting the highest PM_{2.5} levels on the second day of the holiday week, which diverges from the ground truth. This finding suggests that our MAIAC model exhibits a significant enhancement relative to the initial GEOS-CF model in capturing abrupt changes in PM_{2.5} concentrations triggered by extraordinary events, such as holidays, demonstrating its enhanced ability to adapt to dynamic emission patterns.

3.5. Resolution enhancement evaluation

To evaluate the resolution enhancement achieved by our model, Fig. 6 illustrates the comparisons between the first-day PM_{2.5} forecasts at 1 km resolution derived from our MAIAC model with the RF convolutional layer and the first-day PM_{2.5} forecasts at 25 km resolution derived

from the GEOS-CF model on November 20, 2023, for the study domain and three major urban centers in our study area, including the Great Bay Area (GBA) of China, Hangzhou City, and Nanchang City. Fig. 6a and b shows that in terms of the entire study region, the patterns of PM_{2.5} levels forecasted by the two models are comparable. For instance, elevated PM_{2.5} levels are mainly concentrated in large urban areas such as Hangzhou city and the GBA region, whereas lower concentrations are primarily found in rural regions. These findings align closely with land cover patterns, suggesting a relationship between PM_{2.5} concentrations and different land cover types (Mao et al., 2012). However, the 1 km MAIAC forecasts offer significantly more detailed spatial information compared to the 25 km GEOS-CF forecasts. To further showcase the benefits of the enhanced resolution provided by our MAIAC model, we compared the spatial patterns of PM_{2.5} forecasts generated by our MAIAC model to the percentage of impervious surfaces across three urban centers. Compared to the Urban Impervious Surface maps (Fig. 6o-q), MAIAC forecasts at 1 km resolution (Fig. 6c-g,k) reveal a

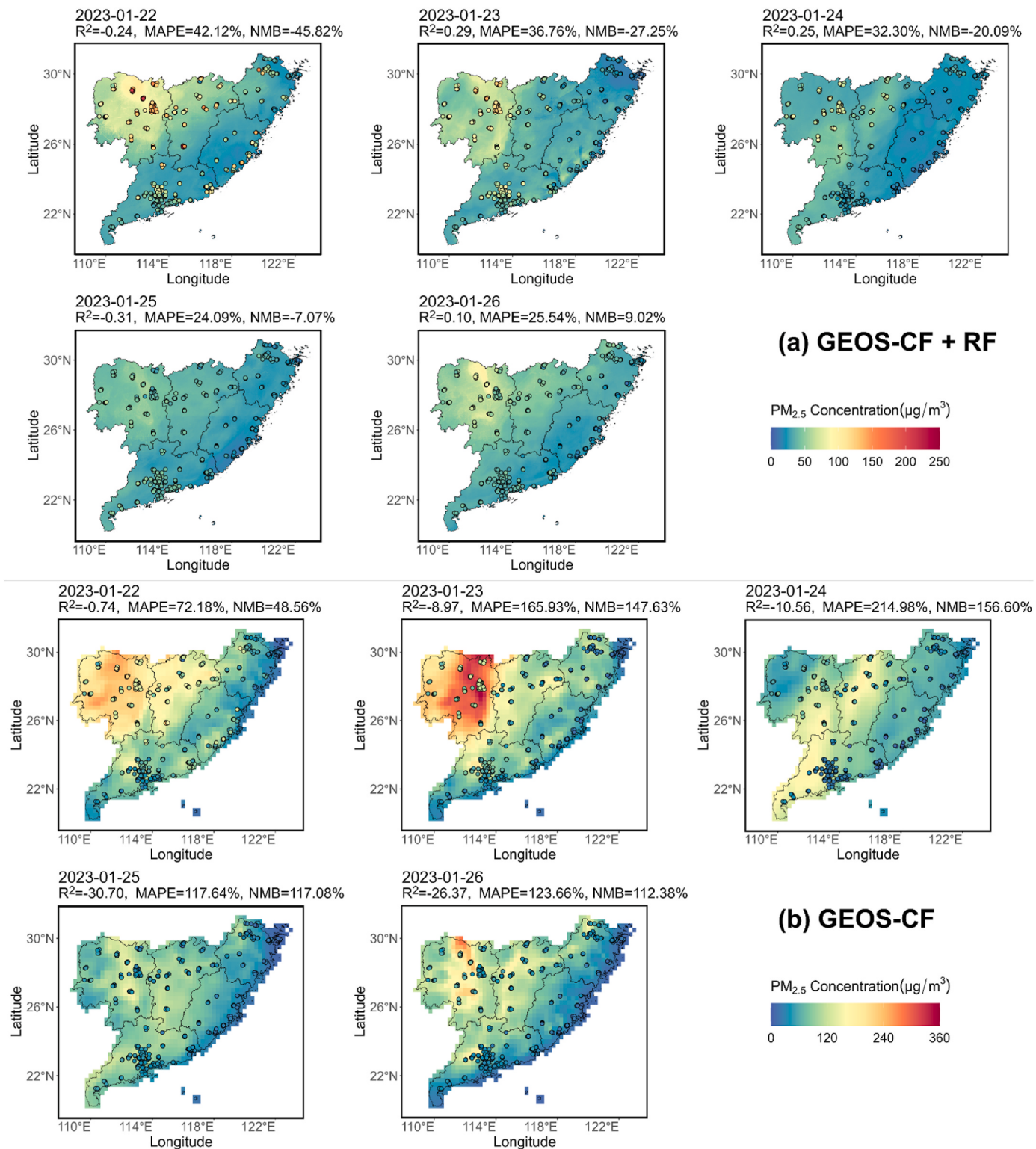


Fig. 5. Spatial distributions of the 5-day PM_{2.5} forecasts derived from (a) our MAIAC model (GEOS-CF + RF) and (b) the GEOS-CF model on January 21, 2023, one day prior to the Lunar New Year holiday week.

strong correlation between elevated PM_{2.5} levels and areas dominated by urban land use, as well as major roads. Conversely, lower PM_{2.5} concentrations are observed in areas with more green spaces, such as parks and rural regions. The 25 km resolution GEOS-CF forecasts (Fig. 6e-i,m) do not provide the spatial detail to identify this trend, primarily due to their relatively coarse resolution, which limits their ability to distinguish between specific land use patterns and their

corresponding PM_{2.5} concentrations. Notably, our 1 km MAIAC forecasts offer significantly higher spatial detail within a 25 km × 25 km GEOS-CF grid cell (Fig. 6d-h,l), allowing for the identification of localized patterns such as elevated PM_{2.5} concentrations near primary roads, which is not possible with the coarser resolution GEOS-CF forecasts (Fig. 6f-j,n). Furthermore, our MAIAC model offers significantly higher accuracy than the GEOS-CF model in forecasting PM_{2.5} levels for the entire 5-day

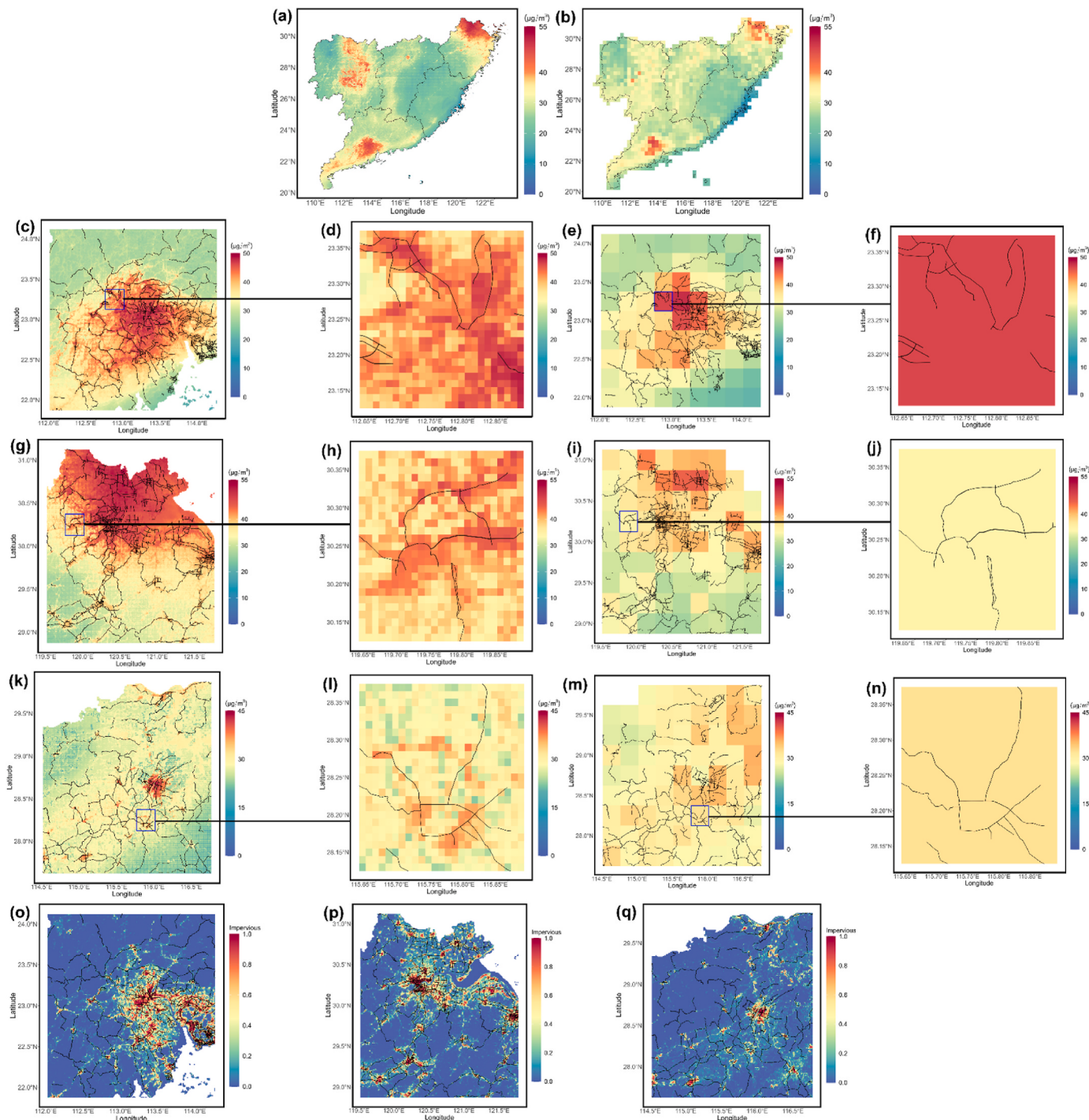


Fig. 6. (a) 1 km $\text{PM}_{2.5}$ forecasts from our MAIAC model for the study area, (b) 25 km $\text{PM}_{2.5}$ forecasts from the GEOS-CF model for the study area, (c) 1 km $\text{PM}_{2.5}$ forecasts from our MAIAC model for the GBA of China, (d) 1 km $\text{PM}_{2.5}$ forecasts within a 25 km \times 25 km grid for the GBA of China, (e) 25 km $\text{PM}_{2.5}$ forecasts from the GEOS-CF model for the GBA of China, (f) 25 km $\text{PM}_{2.5}$ forecasts within a 25 km \times 25 km grid for the GBA of China, (g) 1 km $\text{PM}_{2.5}$ forecasts from our MAIAC model for Hangzhou city, (h) 1 km $\text{PM}_{2.5}$ forecasts within a 25 km \times 25 km grid for Hangzhou city, (i) 25 km $\text{PM}_{2.5}$ forecasts from the GEOS-CF model for Hangzhou city, (j) 25 km $\text{PM}_{2.5}$ forecasts within a 25 km \times 25 km grid for Hangzhou city, (k) 1 km $\text{PM}_{2.5}$ forecasts from our MAIAC model for Nanchang city, (l) 1 km $\text{PM}_{2.5}$ forecasts within a 25 km \times 25 km grid for Nanchang city, (m) 25 km $\text{PM}_{2.5}$ forecasts from the GEOS-CF model for Nanchang city, (n) 25 km $\text{PM}_{2.5}$ forecasts within a 25 km \times 25 km grid for Nanchang city, and urban built-up area for (o) the GBA of China, (p) Hangzhou city, and (q) Nanchang city. (Black lines denote primary roads.)

forecasting period.

3.6. The evaluation of the convolutional layer generated from MAIAC AOD

To quantify the contribution of the convolutional layer to the overall

accuracy of $\text{PM}_{2.5}$ forecasts during the 5-day forecasting period, we evaluated two 1 km model setups for our forecasting framework. These included the model without the RF convolutional layer and our MAIAC model incorporating the RF convolutional layer. Table 4 presents the comparison of overall validation results between these two models. The results show that our MAIAC model delivered more accurate forecasts

for all five forecast days in terms of the validation metrics, outperforming the model lacking the convolutional layer. This finding demonstrated that the RF convolutional layer generated using satellite AOD data played a crucial role in enhancing the accuracy of model forecasts, effectively capturing the spatiotemporal relationships between PM_{2.5} levels on the current and upcoming days. However, the benefits of the convolutional layer to model performance gradually diminished from day one to day five. Table 5 presents the results of a tenfold spatial CV applied to the five-day PM_{2.5} forecasts over the one-year period, and two model configurations were evaluated, comprising the model lacking the convolutional layer and our MAIAC model. The spatial CV outcomes were largely in line with the overall validation, displaying comparable trends in model performance. Our MAIAC model outperformed the model lacking the convolutional layer across all five forecast days. This result suggests that our MAIAC model is capable of delivering significantly more accurate PM_{2.5} forecasts in areas without monitoring sites than the model lacking the convolutional layer.

To evaluate the convolutional layer's effect on the spatial patterns of PM_{2.5} forecasts during the 5-day forecasting period, Fig. 7 showcases the comparisons between the spatial distributions of PM_{2.5} forecasts generated by the model without the convolutional layer and our MAIAC model, respectively. The findings indicate that the model without the convolutional layer (Fig. 7a and b) yielded less accurate forecasts, achieving an R^2 value of 0.48. Furthermore, the spatial pattern of PM_{2.5} forecasts from the model without the convolutional layer (Fig. 7a) fails to distinctly differentiate between urban and rural regions, especially when contrasted with the spatial distribution of impervious surfaces illustrated in Fig. 7g. In contrast, our MAIAC model, illustrated in Fig. 7c and d, substantially outperformed the model lacking the convolutional layer, with an R^2 of 0.66. The spatial pattern of PM_{2.5} forecasts from our MAIAC model exhibits a more pronounced distinction between urban and rural areas, with regions featuring higher percentages of impervious surface typically showing elevated levels of PM_{2.5} concentrations. Likewise, when comparing the spatial distributions of PM_{2.5} forecasts derived from the two models within a 25 km × 25 km pixel depicted in Fig. 7b and d, the result from our MAIAC model exhibits higher contrast between primary roads and non-road areas compared to those from the model lacking the convolutional layer. Both models provide a considerably higher level of spatial detail when compared to the GEOS-CF forecasts (Fig. 7e and f). These findings demonstrate that high-resolution satellite AOD data, when incorporated into the forecast model, could provide extra spatial information with fine details, resulting in more accurate forecasting of spatial patterns of PM_{2.5} levels.

Overall, the results demonstrated that our MAIAC model, integrated with satellite AOD data, significantly outperformed the original GEOS-CF product in terms of forecasting accuracy. This enhanced

Table 4

Comparison of overall validation performance between two models for the period from January 01, 2023 to December 31, 2023.

Forecast day	Model	R^2	RMSE	MAPE (%)	NMB (%)
Day 1	No convolutional layer	0.6159	12.5020	39.69	-0.90
	Our MAIAC	0.7142	10.7841	33.94	-0.21
Day2	No convolutional layer	0.5994	12.7578	40.44	-1.15
	Our MAIAC	0.6407	12.0834	38.53	-0.72
Day3	No convolutional layer	0.5987	12.7187	41.06	-0.94
	Our MAIAC	0.6142	12.4719	40.53	-0.59
Day4	No convolutional layer	0.5895	12.8148	42.23	-0.80
	Our MAIAC	0.5995	12.6580	42.16	-0.50
Day5	No convolutional layer	0.5512	13.2897	43.69	-0.96
	Our MAIAC	0.5591	13.1712	43.70	-0.79

Table 5

Comparison of tenfold spatial CV performance between two models for the period from January 01, 2023 to December 31, 2023.

Forecast day	Model	R^2	RMSE	MAPE (%)	NMB (%)
Day1	No convolutional layer	0.6022	12.7234	41.17	-0.66
	Our MAIAC	0.7011	11.0295	35.45	0.34
Day2	No convolutional layer	0.5866	12.9600	41.85	-0.95
	Our MAIAC	0.6287	12.2826	40.03	-0.15
Day3	No convolutional layer	0.5839	12.9521	42.47	-0.74
	Our MAIAC	0.6014	12.6762	42.93	-0.10
Day4	No convolutional layer	0.5743	13.0491	43.64	-0.56
	Our MAIAC	0.5821	12.9293	43.58	-0.12
Day5	No convolutional layer	0.5384	13.4722	45.05	-0.66
	Our MAIAC	0.5440	13.3954	45.06	-0.50

performance was consistently observed across various validation methods, including overall, site-specific, and day-specific evaluations. Additionally, the 10-fold spatial cross-validation further confirmed the superior performance of our MAIAC model in regions without monitoring stations. Notably, the integration of MAIAC AOD data enabled more precise spatial representations of PM_{2.5} forecasts at high spatial resolution, leading to improved forecasting of spatial patterns.

4. Discussion

This study employed a new forecasting model incorporating ground observations, the GEOS-CF PM_{2.5} forecasts, 1 km resolution MAIAC AOD data, and the random forest model, aiming to enhance the precision of the initial GEOS-CF PM_{2.5} forecasts throughout a 5-day forecasting period at a spatial resolution of 1 km. Although GEOS-CF PM_{2.5} forecasts moderately correlate with ground measurements, this study highlights its significant systematic biases and poor spatial resolution, indicating a need for further refinement to improve accuracy and resolution. GEOS-CF often overestimates ground-level PM_{2.5} concentrations, with the largest discrepancies occurring in Asia (Keller et al., 2021). Our finding corroborates the significant overestimation of PM_{2.5} levels observed in the GEOS-CF data within the referenced study. Our MAIAC model significantly enhances the accuracy of original GEOS-CF PM_{2.5} forecasts for all five forecast days, robustly confirmed through multifaceted validation approaches, including site-specific, overall, and day-specific assessments, underscoring our MAIAC model's reliability and broad applicability. Consistent with the overall validation findings, the spatial CV results confirm our MAIAC model's enhanced accuracy in forecasting PM_{2.5} concentrations, particularly in areas without ground monitoring. In contrast to conventional time-series approaches that rely exclusively on historical data from ground monitoring sites (Zhang et al., 2018; Zhao et al., 2022), our MAIAC model allows for a more inclusive and spatially expansive assessment of air quality dynamics throughout the target area. Although our MAIAC model exhibited diminished forecasting capabilities for PM_{2.5} concentrations in the presence of unanticipated decreases, this model demonstrates superior performance in capturing pollution trends during abrupt events, such as the Lunar New Year holiday week, when compared to the original GEOS-CF dataset. As expected, the performance of both the GEOS-CF model and our forecast model diminished over longer forecast periods. This degradation in accuracy is typical of models trained on historical data, as the relationship between past patterns and future outcomes becomes less reliable over extended time horizons (Qi et al., 2019). Overall, our findings highlight the feasibility and importance of using machine learning and high-resolution satellite AOD data to improve the precision and resolution of CTM forecasting outcomes, enabling the generation of precise

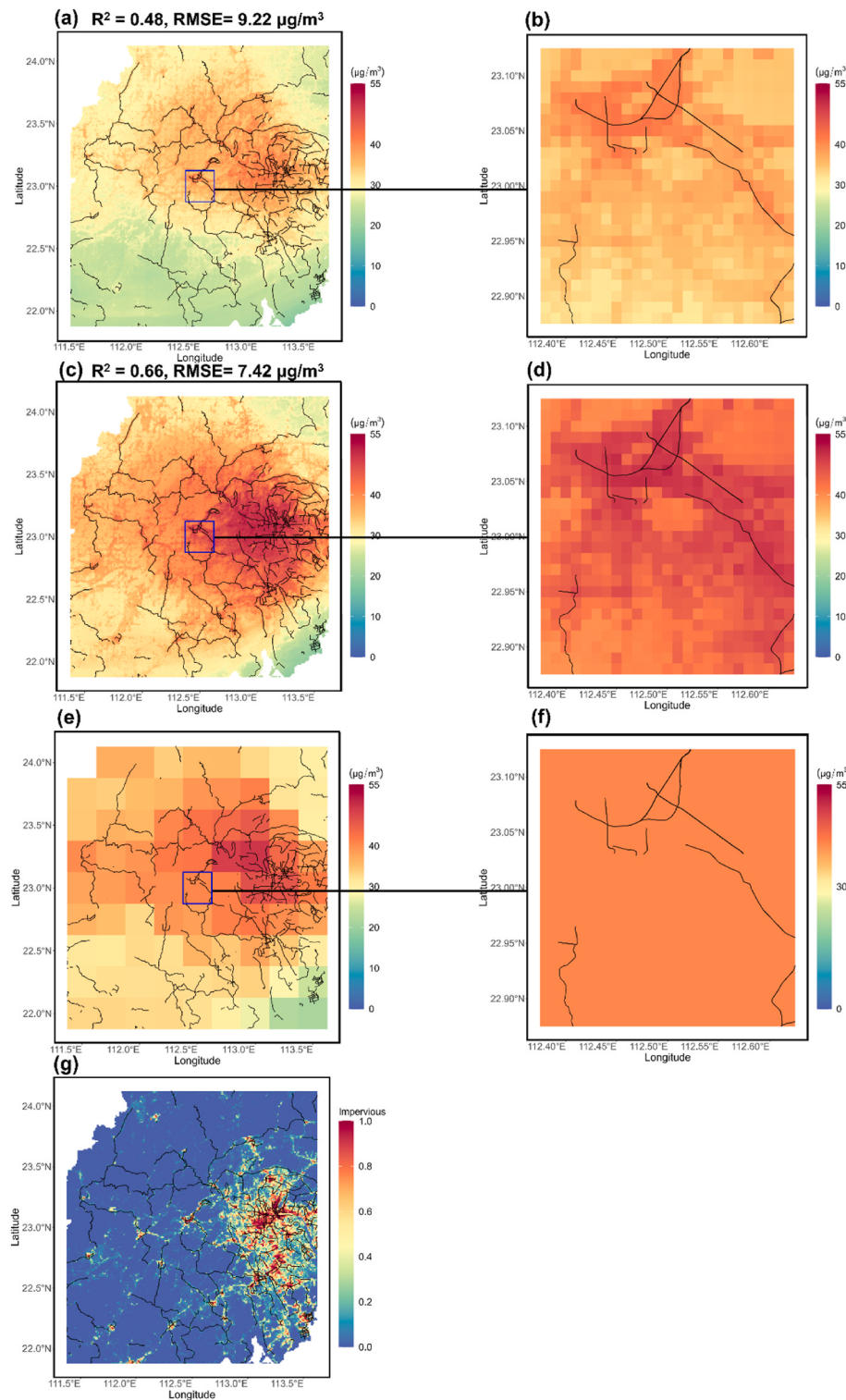


Fig. 7. (a) 1 km $\text{PM}_{2.5}$ forecasts from the model with no convolutional layer, (b) 1 km $\text{PM}_{2.5}$ forecasts from the model with no convolutional layer within a 25 km × 25 km grid, (c) 1 km $\text{PM}_{2.5}$ forecasts from our MAIAC model, (d) 1 km $\text{PM}_{2.5}$ forecasts from our MAIAC model within a 25 km × 25 km grid, (e) 25 km $\text{PM}_{2.5}$ forecasts from the GEOS-CF model, (f) 25 km $\text{PM}_{2.5}$ forecasts from the GEOS-CF model within a 25 km × 25 km grid, and (g) urban built-up area. (Black lines denote primary roads.)

$\text{PM}_{2.5}$ forecasts at fine resolutions.

This study constructed a $\text{PM}_{2.5}$ forecasting framework using 1 km resolution MAIAC AOD data and achieved a high resolution of 1 km for $\text{PM}_{2.5}$ forecasts. 1 km-resolution $\text{PM}_{2.5}$ forecasts offer significantly greater spatial detail compared to 25 km forecasts, providing accurate predictions within 1 km × 1 km grid cells. High-resolution forecasts of

$\text{PM}_{2.5}$ levels can greatly improve the management of air pollution control, particularly during periods of elevated pollution events (Wu et al., 2023). In addition, this detailed information allows for a more precise assessment of population exposure to air pollution, providing valuable insights into the health risks associated with specific microenvironments. As a result, the high spatial resolution of these forecasting data

makes them particularly valuable for research in environmental health, as epidemiological studies often rely on health data from localized, small-scale geographic areas (Hu et al., 2014).

To assess the benefits of the convolutional layer in PM_{2.5} forecasting, this study compared two model configurations, comprising our MAIAC model and the model without the convolutional layer. Both the spatial CV and the overall validation demonstrated that the model with no convolutional layers exhibited lower accuracy than our MAIAC model for all five forecasting days, indicating the substantial contribution of the convolutional layer to accurate PM_{2.5} forecasting. Model improvements attributed to the convolutional layer became progressively less significant across the five-day forecasting period. This is expected because the correlation between present-day PM_{2.5} values and future-day PM_{2.5} values likely weakens over time. Our results further suggested that the RF convolutional layer is effective at capturing spatial patterns in PM_{2.5} levels, possibly due to the incorporation of additional spatial information like high-resolution satellite AOD data. Earlier research revealed that the correlations between PM_{2.5} and AOD ranged from moderate to high, with the strength of the association varying significantly depending on the specific location and time of the year (Engel-Cox et al., 2004; Guo et al., 2017; Li et al., 2015; Wang and Christopher, 2003). Prior research has highlighted the importance of AOD data for enhancing the precision and resolution of PM_{2.5} predictions (Hu et al., 2014, 2017). The findings of this study further underscored the potential of utilizing high-resolution satellite AOD data to enhance the accuracy and spatial resolution of PM_{2.5} concentration forecasts for the upcoming five days.

The inclusion of historic PM_{2.5} measurements from a specific time-frame, known as the rolling period, prior to the forecast date had a considerable impact on the overall effectiveness of the model. Our analysis of different rolling periods showed that using a longer period of historical PM_{2.5} data to train the model generally led to more accurate PM_{2.5} forecasts. This finding aligns closely with previous research (Bi et al., 2022; Li et al., 2025). While longer rolling periods seemed to slightly improve forecasting accuracy, the gains were minimal. On the other hand, using more historical data significantly increased the computation burden. Based on our findings, a 60-day rolling window was deemed optimal. This duration provides a reasonable trade-off between the competing demands of accuracy and computational efficiency.

Our MAIAC model offers a major advantage compared to prior studies. Current methods for forecasting PM_{2.5} levels, including CTMs, time series, and machine learning algorithms, often rely on inaccurate spatial data like spatial interpolation and CTM simulations and provide spatial distributions of PM_{2.5} forecasts with limited accuracy or low resolution. For example, Wu et al. (2020) established a model for bias correction, utilizing the random forest technique, to refine the initial CAMS PM_{2.5} forecast data, resulting in correlation coefficient values of 0.78 for 3-h forecasts and 0.76 for 120-h forecasts. Singh et al. (2024) employed a deep learning approach to enhance the accuracy of 72-h simulation results from the CMAQ model. The framework demonstrated strong performance in four provinces of South Korea, with correlation coefficient values ranging from 0.634 to 0.740, 0.531 to 0.657, and 0.460 to 0.598 for three consecutive days, respectively. Zhao et al. (2025) combined the NAQPMS PM_{2.5} forecasts with a deep learning approach to predict PM_{2.5} concentrations over the following three days, achieving correlation coefficient values of 0.75, 0.62, and 0.55 for the first, second, and third days, respectively. The precision of the forecasts in these studies is either lower or on par with our findings. Notably, they lack the capability to deliver PM_{2.5} forecasts at a spatial resolution as fine as 1 km. This limitation arises because they solely depend on the use of CTM data to provide spatial details. Bi et al. (2022) utilized spatial interpolation to supplement the CTM forecasts with additional spatial information, thereby mitigating inherent biases and enabling the forecasts to be spatially downscaled to a higher resolution of 1 km. Table S2 reveals that the integration of our approach with MAIAC AOD yielded

superior forecast accuracy compared to their model for each of the five forecast days. This limitation arises because spatial interpolation, despite its utility in generating seamless spatial surfaces, inherently smooths over localized fluctuations that are pivotal in elucidating the terrain's impact on air quality dynamics. Furthermore, computational constraints typically restrict the spatial resolution of CTMs, thereby constraining their ability to deliver a nuanced analysis of PM_{2.5} dispersal patterns. Our MAIAC model represents a significant advancement over previous methodologies for forecasting PM_{2.5} concentrations. Its improved accuracy and spatial resolution are achieved through the incorporation of enhanced spatial data, notably high-resolution satellite-derived AOD measurements.

Our method has several constraints. First, our MAIAC model's performance in forecasting PM_{2.5} concentrations weakened when confronted with unanticipated decreases, likely resulting from external variables not considered in our study's boundaries, such as the transport of PM_{2.5} pollution from adjacent provinces and pollution dilution due to clean air brought by strong south and east winds from the ocean. While machine learning models offer promising capabilities, their ability to capture the dynamic changes in PM_{2.5} levels associated with sudden events is limited without incorporating additional relevant factors during training. One potential solution to this problem is to integrate data from regional CTMs that offer high spatial resolution, like the CMAQ model. Second, the static nature of our land-use variables is a limitation, potentially hindering the model's ability to accurately predict PM_{2.5} fluctuations caused by the long-range transport of pollutants and consequently reducing overall predictive power. While MAIAC-based convolutional layers offer a means to capture spatial and temporal PM_{2.5} variations, incorporating dynamic indicators like Normalized Difference Vegetation Index (NDVI) in place of static vegetation data could better reflect temporal changes. Further research is essential to minimize this uncertainty and enhance model performance. Third, while ordinary kriging is used to interpolate GEOS-CF PM_{2.5} and meteorological forecasts to a 1 km resolution, the resulting data may not fully capture localized variations influenced by terrain. Although the resulting interpolation uncertainty is likely to be less significant than the uncertainties inherent in the initial GEOS-CF model, reducing this interpolation uncertainty remains a crucial area for further research and improvement. Finally, our forecasting framework was designed to work in a near-real-time mode, which requires the collection of all related data at the end of the day before executing the forecasting model. However, there is a potential time lag associated with the availability of the MAIAC AOD product. MAIAC AOD data, with its 1 km spatial resolution, was selected in this study to demonstrate the feasibility of employing 1 km resolution satellite AOD data to generate 1 km resolution PM_{2.5} forecasts. As satellite AOD products continue to expand, an increasing number of high-spatiotemporal resolution AOD products are becoming available for forecasting PM_{2.5}. These products deliver real-time observations of pollution distributions, offering significantly broader spatiotemporal coverage compared to ground-based measurements (Teng et al., 2023). For example, the Sentinel-5P TROPOspheric Monitoring Instrument (TROPOMI) provides near-real-time (NRTI) O₃ and NO₂ data, which becomes available within 3 h after the measurements (Garane et al., 2019). These data can be potentially employed to produce near-real-time high-resolution NO₂ and ozone forecasts using the approach proposed by this study.

5. Conclusions

This study presented a novel approach to demonstrate the feasibility of employing 1 km resolution satellite AOD data to generate 1 km resolution PM_{2.5} forecasts in southeastern China over a five-day forecasting horizon by integrating MAIAC AOD measurements into a machine learning forecast model. Based on our findings, we can identify two key conclusions: (1) Our MAIAC model integrated with satellite AOD outperformed the initial GEOS-CF model and can better capture the

complex dynamics of PM_{2.5} pollution in our study domain; (2) incorporating high-resolution satellite AOD into the forecasting model could improve the overall accuracy and spatial resolution of PM_{2.5} forecasts. It is expected that the proposed forecasting framework can adapt to other geographic locations and different air pollutants, such as NO₂ and O₃. The insights from this study can empower environmental agencies in China to implement effective measures to combat PM_{2.5} pollution.

CRediT authorship contribution statement

Zeyue Li: Writing – original draft, Visualization, Validation, Software, Investigation, Formal analysis, Data curation. **Yang Liu:** Writing – review & editing, Methodology. **Jianzhao Bi:** Writing – review & editing, Methodology. **Xuefei Hu:** Writing – review & editing, Supervision, Resources, Project administration, Methodology, Investigation, Funding acquisition, Conceptualization.

Declaration of competing interest

The authors declare that they have no known competing financial interests or personal relationships that could have appeared to influence the work reported in this paper.

Appendix A. Supplementary data

Supplementary data to this article can be found online at <https://doi.org/10.1016/j.jclepro.2025.146759>.

Data availability

Data will be made available on request.

References

- Abuoulezz, W., Ali, N., Aung, Z., Altunaiji, A., Shah, S.B., Gliddon, D., 2025. Exploring PM_{2.5} and PM10 ML forecasting models: a comparative study in the UAE. *Sci. Rep.* 15, 9797.
- Ameri, R., Hsu, C.-C., Band, S.S., Zamani, M., Shu, C.-M., Khorsandroo, S., 2023. Forecasting PM 2.5 concentration based on integrating of CEEMDAN decomposition method with SVM and LSTM. *Ecotoxicol. Environ. Saf.* 266, 115572.
- Apte, J.S., Brauer, M., Cohen, A.J., Ezzati, M., Pope III, C.A., 2018. Ambient PM_{2.5} reduces global and regional life expectancy. *Environ. Sci. Technol. Lett.* 5, 546–551.
- Bi, J., Knowland, K.E., Keller, C.A., Liu, Y., 2022. Combining machine learning and numerical simulation for high-resolution PM_{2.5} concentration forecast. *Environ. Sci. Technol.* 56, 1544–1556.
- Cao, Q., Rui, G., Liang, Y., 2018. Study on PM_{2.5} pollution and the mortality due to lung cancer in China based on geographic weighted regression model. *BMC Public Health* 18, 925.
- Chang, Y.-Y., Chiao, H.-T., Abimannan, S., Huang, Y.-P., Tsai, Y.-T., Lin, K.-M., 2020. An LSTM-Based aggregated model for air pollution forecasting. *Atmos. Pollut. Res.* 11, 1451–1463.
- Chen, D., Xia, L., Guo, X., Lang, J., Zhou, Y., Wei, L., Fu, X., 2021. Impact of inter-annual meteorological variation from 2001 to 2015 on the contribution of regional transport to PM_{2.5} in Beijing, China. *Atmos. Environ.* 260, 118545.
- Cheng, F.-Y., Feng, C.-Y., Yang, Z.-M., Hsu, C.-H., Chan, K.-W., Lee, C.-Y., Chang, S.-C., 2021. Evaluation of real-time PM_{2.5} forecasts with the WRF-CMAQ modeling system and weather-pattern-dependent bias-adjusted PM_{2.5} forecasts in Taiwan. *Atmos. Environ.* 244, 117909.
- Cohen, A.J., Brauer, M., Burnett, R., Anderson, H.R., Fostad, J., Estep, K., Balakrishnan, K., Brunekreef, B., Dandona, L., Dandona, R., Feigin, V., Freedman, G., Hubbell, B., Jobling, A., Kan, H., Knibbs, L., Liu, Y., Martin, R., Morawska, L., Pope III, C.A., Shin, H., Straif, K., Shaddick, G., Thomas, M., van Dingenen, R., van Donkelaar, A., Vos, T., Murray, C.J.L., Forouzanfar, M.H., 2017. Estimates and 25-year trends of the global burden of disease attributable to ambient air pollution: an analysis of data from the global burden of diseases study 2015. *Lancet* 389, 1907–1918.
- Engel-Cox, J.A., Holloman, C.H., Coutant, B.W., Hoff, R.M., 2004. Qualitative and quantitative evaluation of MODIS satellite sensor data for regional and urban scale air quality. *Atmos. Environ.* 38, 2495–2509.
- Feng, R., Zheng, H.-j., Gao, H., Zhang, A.-r., Huang, C., Zhang, J.-x., Luo, K., Fan, J.-r., 2019. Recurrent neural network and random forest for analysis and accurate forecast of atmospheric pollutants: a case study in hangzhou, China. *J. Clean. Prod.* 231, 1005–1015.
- Feng, X., Zhang, X., Henne, S., Zhao, Y.-B., Liu, J., Chen, T.-L., Wang, J., 2024. A hybrid model for enhanced forecasting of PM_{2.5} spatiotemporal concentrations with high resolution and accuracy. *Environ. Pollut.* 355, 124263.
- Gao, Z., Zhou, X., 2024. A review of the CAMx, CMAQ, WRF-chem and NAQPMS models: application, evaluation and uncertainty factors. *Environ. Pollut.* 343, 123183.
- Garane, K., Koukouli, M.E., Verhoelst, T., Lerot, C., Heue, K.P., Fioletov, V., Balis, D., Bais, A., Bazireau, A., Dehn, A., Goutail, F., Granville, J., Griffin, D., Hubert, D., Keppens, A., Lambert, J.C., Loyola, D., McLinden, C., Pazmino, A., Pommereau, J.P., Redondas, A., Romahn, F., Valks, P., Van Roozendael, M., Xu, J., Zehner, C., Zerefos, C., Zimmer, W., 2019. TROPOMI/SSP total ozone column data: global ground-based validation and consistency with other satellite missions. *Atmos. Meas. Tech.* 12, 5263–5287.
- Gualtieri, G., Brilli, L., Carotenuto, F., Cavalieri, A., Gioli, B., Giordano, T., Putzolu, S., Vagnoli, C., Zaldei, A., 2025. Assessing capability of copernicus atmosphere monitoring service to forecast PM_{2.5} and PM10 hourly concentrations in a European air quality hotspot. *Atmos. Pollut. Res.* 16, 102567.
- Guo, J., Xia, F., Zhang, Y., Liu, H., Li, J., Lou, M., He, J., Yan, Y., Wang, F., Min, M., Zhai, P., 2017. Impact of diurnal variability and meteorological factors on the PM_{2.5} - AOD relationship: implications for PM_{2.5} remote sensing. *Environ. Pollut.* 221, 94–104.
- Handschuh, J., Erbertseder, T., Baier, F., 2024. On the added value of satellite AOD for the investigation of ground-level PM_{2.5} variability. *Atmos. Environ.* 331, 120601.
- Hayes, R.B., Lim, C., Zhang, Y., Cromar, K., Shao, Y., Reynolds, H.R., Silverman, D.T., Jones, R.R., Park, Y., Jerrett, M., Ahn, J., Thurston, G.D., 2019. PM_{2.5} air pollution and cause-specific cardiovascular disease mortality. *Int. J. Epidemiol.* 49, 25–35.
- He, Q., Ye, T., Wang, W., Luo, M., Song, Y., Zhang, M., 2023. Spatiotemporally continuous estimates of daily 1-km PM_{2.5} concentrations and their long-term exposure in China from 2000 to 2020. *J. Environ. Manag.* 342, 118145.
- Hu, X., Belle, J.H., Meng, X., Wildani, A., Waller, L.A., Strickland, M.J., Liu, Y., 2017. Estimating PM_{2.5} concentrations in the conterminous United States using the random forest approach. *Environ. Sci. Technol.* 51, 6936–6944.
- Hu, X., Waller, L.A., Al-Hamdan, M.Z., Crosson, W.L., Estes, M.G., Estes, S.M., Quattrochi, D.A., Sarnat, J.A., Liu, Y., 2013. Estimating ground-level PM_{2.5} concentrations in the southeastern U.S. using geographically weighted regression. *Environ. Res.* 121, 1–10.
- Hu, X., Waller, L.A., Lyapustina, A., Wang, Y., Al-Hamdan, M.Z., Crosson, W.L., Estes, M.G., Estes, S.M., Quattrochi, D.A., Puttaswamy, S.J., Liu, Y., 2014. Estimating ground-level PM_{2.5} concentrations in the southeastern United States using MAIAC AOD retrievals and two-stage model. *Rem. Sens. Environ.* 140, 220–232.
- Hu, Y., Li, Q., Shi, X., Yan, J., Chen, Y., 2024. Domain knowledge-enhanced multi-spatial multi-temporal PM_{2.5} forecasting with integrated monitoring and reanalysis data. *Environ. Int.* 192, 108997.
- Huang, G., Li, X., Zhang, B., Ren, J., 2021. PM_{2.5} concentration forecasting at surface monitoring sites using GRU neural network based on empirical mode decomposition. *Sci. Total Environ.* 768, 144516.
- Jena, C., Ghude, S.D., Kumar, R., Debnath, S., Govardhan, G., Soni, V.K., Kulkarni, S.H., Beig, G., Nanjundiah, R.S., Rajeevan, M., 2021. Performance of high resolution (400 m) PM_{2.5} forecast over Delhi. *Sci. Rep.* 11, 4104.
- Jin, X., Fiore, A.M., Civerolo, K., Bi, J., Liu, Y., van Donkelaar, A., Martin, R.V., Al-Hamdan, M., Zhang, Y., Insaf, T.Z., Kioumourtzoglou, M.-A., He, M.Z., Kinney, P.L., 2019. Comparison of multiple PM_{2.5} exposure products for estimating health benefits of emission controls over New York state, USA. *Environ. Res. Lett.* 14, 084023.
- Keller, C.A., Knowland, K.E., Duncan, B.N., Liu, J., Anderson, D.C., Das, S., Lucchesi, R.A., Lundgren, E.W., Nicely, J.M., Nielsen, E., Ott, L.E., Saunders, E., Strode, S.A., Wales, P.A., Jacob, D.J., Pawson, S., 2021. Description of the NASA GEOS composition forecast modeling system GEOS-CF v1.0. *J. Adv. Model. Earth Syst.* 13, e2020MS002413.
- Knowland, K.E., Keller, C.A., Wales, P.A., Wargan, K., Coy, L., Johnson, M.S., Liu, J., Lucchesi, R.A., Eastham, S.D., Fleming, E., Liang, Q., Leblanc, T., Livesey, N.J., Walker, K.A., Ott, L.E., Pawson, S., 2022. NASA GEOS composition forecast modeling system GEOS-CF v1.0: stratospheric composition. *J. Adv. Model. Earth Syst.* 14, e2021MS002852.
- Kow, P.-Y., Wang, Y.-S., Zhou, Y., Kao, I.F., Issermann, M., Chang, L.-C., Chang, F.-J., 2020. Seamless integration of convolutional and back-propagation neural networks for regional multi-step-ahead PM_{2.5} forecasting. *J. Clean. Prod.* 261, 121285.
- Lee, Y.-J., Cheng, F.-Y., Chien, H.-C., Lin, Y.-C., Sun, M.-T., 2024. Enhancing real-time PM_{2.5} forecasts: a hybrid approach of WRF-CMAQ model and CNN algorithm. *Atmos. Environ.* 338, 120835.
- Li, J., Carlson, B.E., Lacis, A.A., 2015. How well do satellite AOD observations represent the spatial and temporal variability of PM_{2.5} concentration for the United States? *Atmos. Environ.* 102, 260–273.
- Li, Z., Bi, J., Liu, Y., Hu, X., 2025. Forecasting O₃ and NO₂ concentrations with spatiotemporally continuous coverage in southeastern China using a machine learning approach. *Environ. Int.* 195, 109249.
- Liao, Q., Zhu, M., Wu, L., Wang, D., Wang, Z., Zhang, S., Cao, W., Pan, X., Li, J., Tang, X., Xin, J., Sun, Y., Zhu, J., Wang, Z., 2024. Probing the capacity of a spatiotemporal deep learning model for short-term PM_{2.5} forecasts in a coastal urban area. *Sci. Total Environ.* 950, 175233.
- Lin, C.-H., Ryu, J., Choi, Y., Jeon, S.W., Lee, W.-K., 2020. Understanding global PM_{2.5} concentrations and their drivers in recent decades (1998–2016). *Environ. Int.* 144, 106011.
- Lin, M.-D., Liu, P.-Y., Huang, C.-W., Lin, Y.-H., 2024. The application of strategy based on LSTM for the short-term prediction of PM_{2.5} in city. *Sci. Total Environ.* 906, 167892.
- Liu, B.-C., Binaykia, A., Chang, P.-C., Tiwari, M.K., Tsao, C.-C., 2017. Urban air quality forecasting based on multi-dimensional collaborative support vector regression (SVR): a case study of beijing-tianjin-shijiazhuang. *PLoS One* 12, e0179763.
- Lu, X., Sha, Y.H., Li, Z., Huang, Y., Chen, W., Chen, D., Shen, J., Chen, Y., Fung, J.C.H., 2021. Development and application of a hybrid long-short term memory – three

- dimensional variational technique for the improvement of PM2.5 forecasting. *Sci. Total Environ.* 770, 144221.
- Lyapustin, A., Martonchik, J., Wang, Y., Laszlo, I., Korkin, S., 2011a. Multiangle implementation of atmospheric correction (MAIAC): 1. Radiative transfer basis and look-up tables. *J. Geophys. Res. Atmos.* 116.
- Lyapustin, A., Wang, Y., Laszlo, I., Kahn, R., Korkin, S., Remer, L., Levy, R., Reid, J.S., 2011b. Multiangle implementation of atmospheric correction (MAIAC): 2. Aerosol algorithm. *J. Geophys. Res. Atmos.* 116.
- Ma, Z., Hu, X., Huang, L., Bi, J., Liu, Y., 2014. Estimating ground-level PM2.5 in China using satellite remote sensing. *Environ. Sci. Technol.* 48, 7436–7444.
- Mao, L., Qiu, Y., Kusano, C., Xu, X., 2012. Predicting regional space-time variation of PM2.5 with land-use regression model and MODIS data. *Environ. Sci. Pollut. Control Ser.* 19, 128–138.
- Peng, J., Han, H., Yi, Y., Huang, H., Xie, L., 2022. Machine learning and deep learning modeling and simulation for predicting PM2.5 concentrations. *Chemosphere* 308, 136353.
- Qi, Y., Li, Q., Karimian, H., Liu, D., 2019. A hybrid model for spatiotemporal forecasting of PM2.5 based on graph convolutional neural network and long short-term memory. *Sci. Total Environ.* 664, 1–10.
- Singh, D., Choi, Y., Park, J., Salman, A.K., Sayeed, A., Song, C.H., 2024. Deep-BCSI: a deep learning-based framework for bias correction and spatial imputation of PM2.5 concentrations in South Korea. *Atmos. Res.* 301, 107283.
- Stafoggia, M., Bellander, T., Bucci, S., Davoli, M., de Hoogh, K., de' Donato, F., Gariazzo, C., Lyapustin, A., Michelozzi, P., Renzi, M., Scorticichini, M., Shtain, A., Viegi, G., Kloog, I., Schwartz, J., 2019. Estimation of daily PM10 and PM2.5 concentrations in Italy, 2013–2015, using a spatiotemporal land-use random-forest model. *Environ. Int.* 124, 170–179.
- Teng, M., Li, S., Xing, J., Fan, C., Yang, J., Wang, S., Song, G., Ding, Y., Dong, J., Wang, S., 2023. 72-hour real-time forecasting of ambient PM2.5 by hybrid graph deep neural network with aggregated neighborhood spatiotemporal information. *Environ. Int.* 176, 107971.
- Teng, M., Li, S., Yang, J., Chen, J., Fan, C., Ding, Y., 2024. A new hybrid deep neural network for multiple sites PM2.5 forecasting. *J. Clean. Prod.* 473, 143542.
- Wang, J., Christopher, S.A., 2003. Intercomparison between satellite-derived aerosol optical thickness and PM2.5 mass: implications for air quality studies. *Geophys. Res. Lett.* 30.
- Wei, J., Li, Z., Lyapustin, A., Sun, L., Peng, Y., Xue, W., Su, T., Cribb, M., 2021. Reconstructing 1-km-resolution high-quality PM2.5 data records from 2000 to 2018 in China: spatiotemporal variations and policy implications. *Rem. Sens. Environ.* 252, 112136.
- Wei, J., Li, Z., Lyapustin, A., Wang, J., Dubovik, O., Schwartz, J., Sun, L., Li, C., Liu, S., Zhu, T., 2023. First close insight into global daily gapless 1 km PM2.5 pollution, variability, and health impact. *Nat. Commun.* 14, 8349.
- Wu, C., Li, K., Bai, K., 2020. Validation and calibration of CAMS PM2.5 forecasts using in situ PM2.5 measurements in China and United States. *Remote Sens.* 12, 3813.
- Wu, K.-Y., Hsia, I.W., Kow, P.-Y., Chang, L.-C., Chang, F.-J., 2023. High-spatiotemporal-resolution PM2.5 forecasting by hybrid deep learning models with ensembled massive heterogeneous monitoring data. *J. Clean. Prod.* 433, 139825.
- Xiao, Q., Wang, Y., Chang, H.H., Meng, X., Geng, G., Lyapustin, A., Liu, Y., 2017. Full-coverage high-resolution daily PM2.5 estimation using MAIAC AOD in the yangtze river Delta of China. *Rem. Sens. Environ.* 199, 437–446.
- Xing, J., Zheng, S., Li, S., Huang, L., Wang, X., Kelly, J.T., Wang, S., Liu, C., Jang, C., Zhu, Y., Zhang, J., Bian, J., Liu, T.-Y., Hao, J., 2022. Mimicking atmospheric photochemical modeling with a deep neural network. *Atmos. Res.* 265, 105919.
- Yang, J., Yan, R., Nong, M., Liao, J., Li, F., Sun, W., 2021a. PM2.5 concentrations forecasting in beijing through deep learning with different inputs, model structures and forecast time. *Atmos. Pollut. Res.* 12, 101168.
- Yang, X., Zhang, L., Chen, X., Liu, F., Shan, A., Liang, F., Li, X., Wu, H., Yan, M., Ma, Z., Dong, G., Liu, Y., Chen, J., Wang, T., Zhao, B., Liu, Y., Gu, D., Tang, N., 2021b. Long-term exposure to ambient PM2.5 and stroke mortality among urban residents in northern China. *Ecotoxicol. Environ. Saf.* 213, 112063.
- Yu, C., Di Girolamo, L., Chen, L., Zhang, X., Liu, Y., 2015. Statistical evaluation of the feasibility of satellite-retrieved cloud parameters as indicators of PM2.5 levels. *J. Expo. Sci. Environ. Epidemiol.* 25, 457–466.
- Zhang, L., Lin, J., Qiu, R., Hu, X., Zhang, H., Chen, Q., Tan, H., Lin, D., Wang, J., 2018. Trend analysis and forecast of PM2.5 in fuzhou, China using the ARIMA model. *Ecol. Indic.* 95, 702–710.
- Zhang, L., Wilson, J.P., Zhao, N., Zhang, W., Wu, Y., 2022. The dynamics of cardiovascular and respiratory deaths attributed to long-term PM2.5 exposures in global megacities. *Sci. Total Environ.* 842, 156951.
- Zhao, L., Li, Z., Qu, L., 2022. Forecasting of beijing PM2.5 with a hybrid ARIMA model based on integrated AIC and improved GS fixed-order methods and seasonal decomposition. *Heliyon*, 8, e12239.
- Zhao, Z., Wu, H., Chen, K., Kong, L., Tang, X., 2025. Improving the spatiotemporal forecasting of PM2.5 by coupling a deep learning method with a chemical transport model: a severe haze case in China. *Aerosol Science and Engineering*.
- Zheng, H., Liu, J., Tang, X., Wang, Z., Wu, H., Yan, P., Wang, W., 2018. Improvement of the real-time PM2.5 forecast over the beijing-tianjin-hebei region using an optimal interpolation data assimilation method. *Aerosol Air Qual. Res.* 18, 1305–1316.
- Zhou, Y., Chang, F.-J., Chang, L.-C., Kao, I.F., Wang, Y.-S., Kang, C.-C., 2019. Multi-output support vector machine for regional multi-step-ahead PM2.5 forecasting. *Sci. Total Environ.* 651, 230–240.